Supplementary materials for

Replacing Ru complex with carbon dot over MOFs-derived Co_3O_4/In_2O_3 catalyst for efficient solar-driven CO_2 reduction

Qian Liang,[a,*] Xiaotong Yan[a], Zhongyu Li[a], Zhenyu Wu[a], Hong Shi[b], Hui Huang[b] and Zhenhui Kang[b,c,d,*]

[a]Jiangsu Key Laboratory of Advanced Catalytic Materials and Technology, School of Petrochemical Engineering, Changzhou University, Changzhou 213164, China. E-mail: qianliang@cczu.edu.cn

[b]Institute of Functional Nano and Soft Materials Laboratory (FUNSOM), Jiangsu Key Laboratory for Carbon-Based Functional Materials & Devices, Soochow University, Suzhou 215123, China. E-mail: zhkang@suda.edu.cn

[c]Macao Institute of Materials Science and Engineering, Macau University of Science and Technology, Taipa, 999078, Macau SAR, China. E-mail: zhkang@must.edu.mo

[d] Institute of Advanced Materials, Northeast Normal University, Changchun, 130024, China. E-mail: kangzh@nenu.edu.cn

Supplementary Text

1. Experimental section

1.1 Synthesis.

1.1.1 Synthesis of CDs.

The CDs were prepared by a typical electrochemical method. In general, two graphite rods after ultrasonic cleaning were inserted into deionized (DI) water as anode and cathode respectively, and then a 30 V bias was applied between the two electrodes using a direct current power supply. Continue stirring until the stone grinding rod was gradually corroded and the colorless electrolyte turned into a dark solution. The obtained dark solution was filtered and collected by centrifugation, and then freeze-dried to obtain CDs powder. Finally, the CDs powder was dispersed in DI water (0.7 mg mL^{-1}).

1.1.2 Synthesis of In-MIL-68.

Typically, 500 mg $In(NO_3)_3 \cdot xH_2O$ and 500 mg 1,4-benzenedicarboxylic acid were added into 150 mL DMF under stirring for 30 min to form a clear solution. Then, the resulting solution was heated in an oil bath at 120 ℃ for 2 h. Finally, after cooling to room temperature, the white precipitate was collected by centrifugation, washed with ethanol for several times and dried at 60 ℃ for 12 h under vacuum conditions.

1.1.3 Synthesis of ZIF-67/In-MIL-68.

400 mg In-MIL-68 was dissolved in 25 mL methanol and stirred for 10 min to form an off-white suspension. 286 mg of $Co(NO_3)_2 \cdot 6H_2O$ was dissolved in 20 mL methanol, then slowly added to the above solution and stirred for 30 min to form a mixed solution.

652 mg 2-methylimidazole was dissolved in 20 mL methanol and stirred for 10 min until the solution was clear and transparent, and then the solution was added drop by drop to the above mixed solution. After stirred for 24 h, and the products were collected by centrifugation, washed with methanol, and dried in a vacuum oven at 60 ℃ for 12 h. The purple MOF-on-MOF was labeled as ZIF-67/In-MIL-68 (the mass ratio of ZIF-67 to In-MIL-68 was 1:2).

1.1.4 Synthesis of MOF-derived Co_3O_4/In_2O_3.

The prepared ZIF-67/In-MIL-68 composites were put into a tubular furnace, calcined at 120 ℃ for 2 h in air atmosphere with a heating rate of 5 ℃ min^{-1}, and then heated at 550 ℃ for 5 h at the same heating rate to obtain the as-prepared samples. The MOF-derived Co_3O_4/In_2O_3 with the different calcination temperature (500 ^oC, 550 ^oC and 600 ^oC) were labeled as M-Co_3O_4/In_2O_3-x (x=500, 550, 600). Due to the In_2O_3 nanotube with demanding requirements for temperature, calcination temperature should be precisely controlled in a narrow range. ZIF-67 and In-MIL-68 were heated at 550 ^oC under the same condition, respectively, and the resulting samples were denoted as M-Co_3O_4 and M-In_2O_3.

1.1.5 Synthesis of CDs-Co_3O_4/In_2O_3 composites.

The CDs-Co_3O_4/In_2O_3 composites with different mass ratios of CDs (1 wt%, 3 wt% and 5 wt%) were prepared by the following steps. 100 mg Co_3O_4/In_2O_3-550 and carbon dot solutions (1 mg mL^{-1}) with different volume ratios were added to 25 mL DI water by ultrasonic treatment for 30 min, and stirred continuously at room temperature for 24 h. Finally, the product was collected by centrifugation, washed with ethanol for many

times, and then dried in a vacuum drying oven at 60 ℃ for 12 h. The as-synthesized CDs-Co_3O_4/In_2O_3 were abbreviated as x% CDs-M-CIO (x=1, 3, 5).

1.2 Characterization.

The crystalline structures of the CDs-M-CIO composites were analyzed by X-ray diffractometer (XRD, Shimadzu 6000) equipped with Cu Kα radiation. The morphologies and microstructures of the CDs-M-CIO were observed through field emission scanning electron microscopy (FE-SEM, SUPRA55) and transmission electron microscopy (TEM, JEOL 2100). Element mapping was tested by energy dispersive X-ray spectroscopy (EDX) on the same instrument. The Fourier transform infrared (FT-IR) spectrum was performed on a Thermo Fisher FTIR6700 spectrometer at room temperature. Raman spectra was carried out on a Laser Raman spectrometer (LabRAM HR Evolution) with an excitation wavelength of 532 nm. The optical properties of the samples were determined by UV-vis diffuse reflectance spectroscopy (DRS) on a Shimadzu UV-3600 UV-vis spectrophotometer. Steady-state photoluminescence (PL) spectra was measured on a Cary Eclipse fluorescence spectrophotometer at an excitation wavelength of 325 nm. Time-resolved photoluminescence (TRPL) decay spectra was obtained by a FLS1000 fluorescence spectrophotometer. The specific surface area and pore size distribution were collected on a Micromeritics ASAP 2460 analyzer. X-ray photoelectron spectra (XPS) was applied on a Thermo ESCALAB 250 spectrometer with an Al Kα X ray source to examine the chemical states of the samples. Thermogravimetric Analysis (TGA) was measured on a Mettler-Toledo instrument under N_2 atmosphere from room temperature

to 800 ℃. Electron paramagnetic resonance (EPR) measurements were performed with a Bruker EMXPLUS spectrometer.

1.3 Photocatalytic CO_2 Reduction.

The photocatalytic CO_2 reduction was carried out in a 180 mL Pyrex glass reactor at atmospheric pressure under AM1.5 G sunlight simulator. Generally, 10 mg as-prepared sample was added into the mixture solution of MeCN/H_2O by ultrasonic for 30 min, and then degassed and purged with high-purity CO_2. The reaction system was cooled by circulating water to weaken the heating effect and reduce the solvent evaporation rate. The gas was analyzed by GC-7860 Plus gas chromatograph equipped with a thermal conductivity detector (TCD) and a flame ionization detector (FID). The stability of CO_2 reduction was tested by the following cycle experiments: after the reaction, the as-prepared photocatalyst was separated from the reaction solution, washed with DI water, and dried in an oven at 60 ℃ for the next reaction. Under the same condition, two cocatalysts CDs and $[Ru(bpy)_3]Cl_2 \cdot 6H_2O$ were compared to evaluate the photocatalytic CO_2 reduction performance of as-prepared catalysts. Control experiments (with no catalyst, Ar instead of CO_2, or no light) and comparison experiments (using CDs or $[Ru(bpy)_3]Cl_2$ or TEOA in absence of catalyst,) were conducted in the same conditions. ^{13}C-labeled experiment was performed on the same procedure but was also analyzed by gas chromatography-mass spectrometry (GCMS-QP 2020, Shimadzu) for CO production.

1.4 Economic-photocatalytic performances.

CO_2 economic-photocatalytic performances (EP) are calculated by the following equation: EP = (photocatalytic CO generation rate values)/(price of used materials). For instance, the EP without TEOA over Ru-catalyst is equal to 0.64/360=**1.78×10^{-3}** (μmol h^{-1} g^{-1} $\$^{-1}$). Due to the exceptionally low-cost carbon material, the price of CDs is negligible and therefore EP value is equal to the photocatalytic CO generation rate value.

1.5 Photoelectrochemical Performance Measurements.

Photoelectrochemical measurements were obtained on a CHI660D electrochemical workstation with a standard three-electrode system, including a counter electrode (Pt wire), a reference electrode (Ag/AgCl), and a working electrode (FTO glass). Generally, the preparation process of the working electrode was as follows: 2 mg of the as-prepared sample and 75 μL of Nafion were dispersed in 2 mL of ethanol by ultrasonic for 15 min. Then, the above suspension (100 μL) was dropped onto the FTO glass and dried in an oven at 60 °C and Na_2SO_4 (0.5 M) aqueous solution was used as electrolyte. 1 M KOH aqueous solution was used as the electrolyte for the OER experiment. Prior to the experiment, the electrolyte was saturated with O_2 for 30 min roughly and kept under an O_2 atmosphere throughout the whole electrochemical experiment. Linear sweep voltammetry (LSV) curves were obtained at a scan rate of 5 mV s^{-1} from 0 to 0.8 V *versus* Ag/AgCl (3.5 M KCl) to obtain the polarization curves.

1.6 The experimental method of transient photovoltage (TPV).

The TPV measurements were conducted on films samples (1.5 cm × 4 cm) deposited on indium-tin oxide (ITO) glass substrates at room temperature. A 10 mg mL^{-1} sample

aqueous solution was dripped on the ITO substrate, and then dried in air to obtain the films samples. The working electrode (ITO glass modified with samples) and the counter electrode (Pt wire) were wetted with N_2 or O_2-saturated acetonitrile and N_2-saturated acetonitrile/water aqueous (0.5 vol%). Meanwhile, we also measured the powder samples, which were covered on the Pt network (1 cm × 1 cm). The samples were excited by a third-harmonic Nd: YAG laser (Polaris II, New Wave Research, Inc.) with a laser radiation pulse (wavelength 355 nm, pulse width 5 ns).

Supplementary Figures

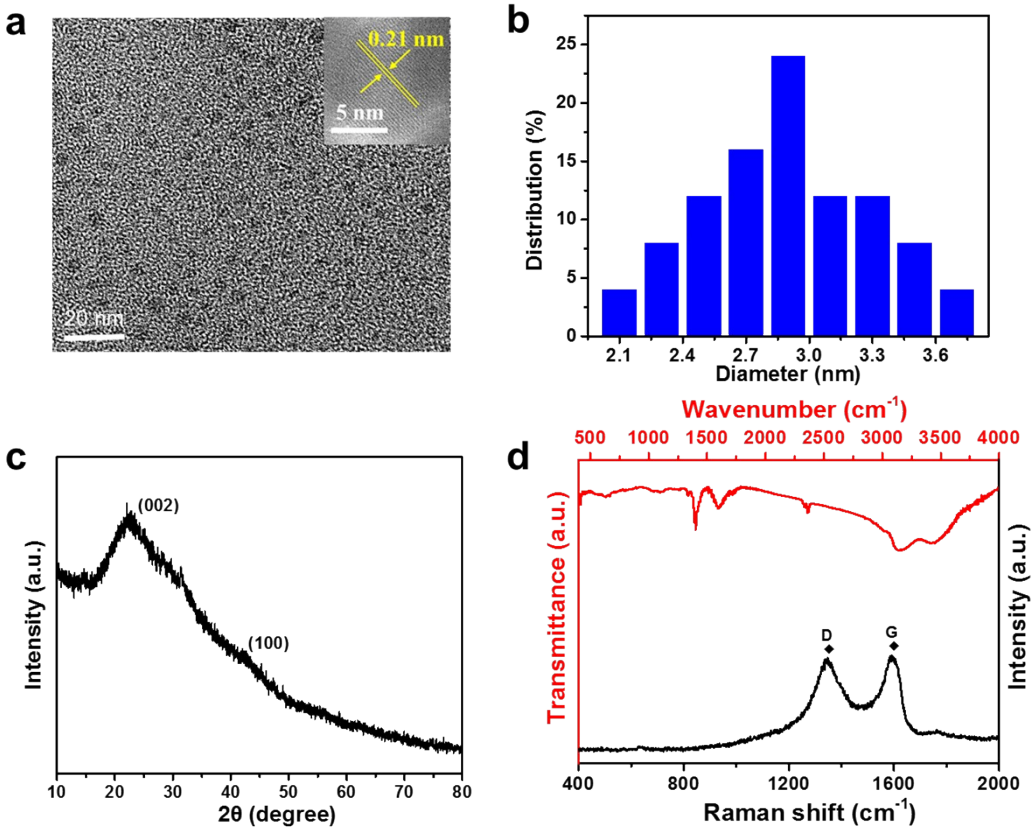

Fig. S1 (a) TEM image, (b) size distribution, (c) XRD pattern, (d) Raman and FT-IR spectra of CDs.

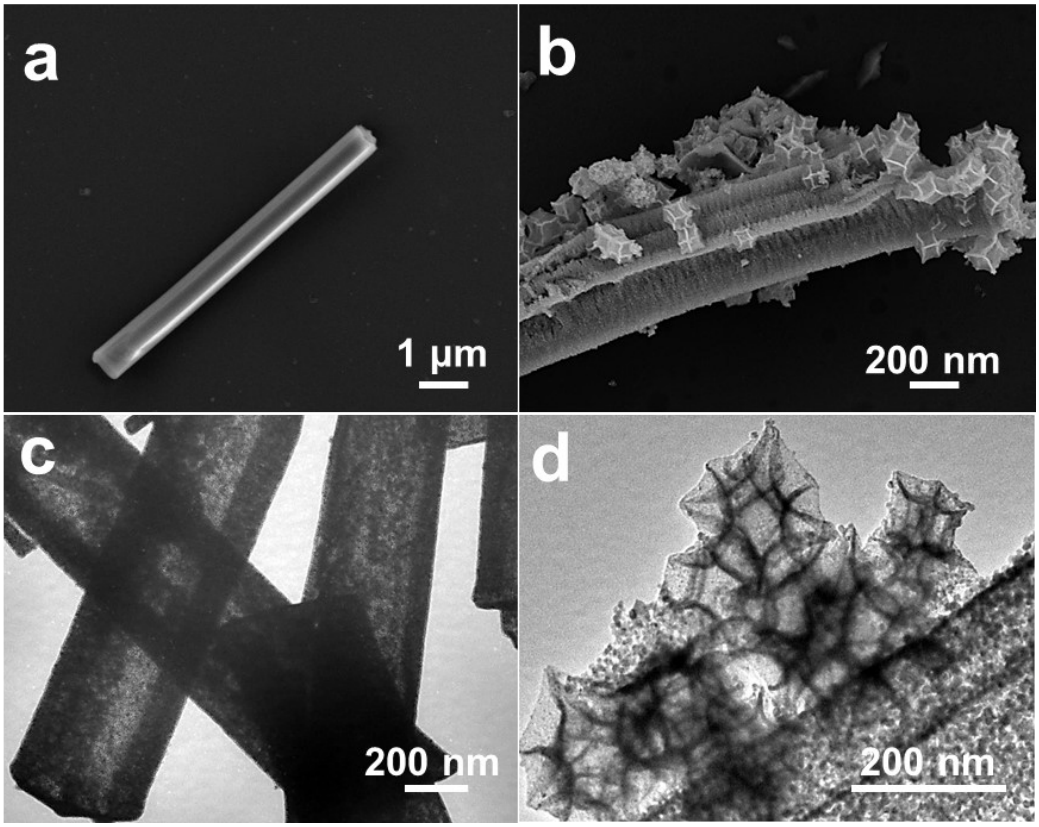

Fig. S2 (a, c) SEM and TEM images of M-In_2O_3. (b, d) SEM and TEM images of 3% CDs-M-CIO.

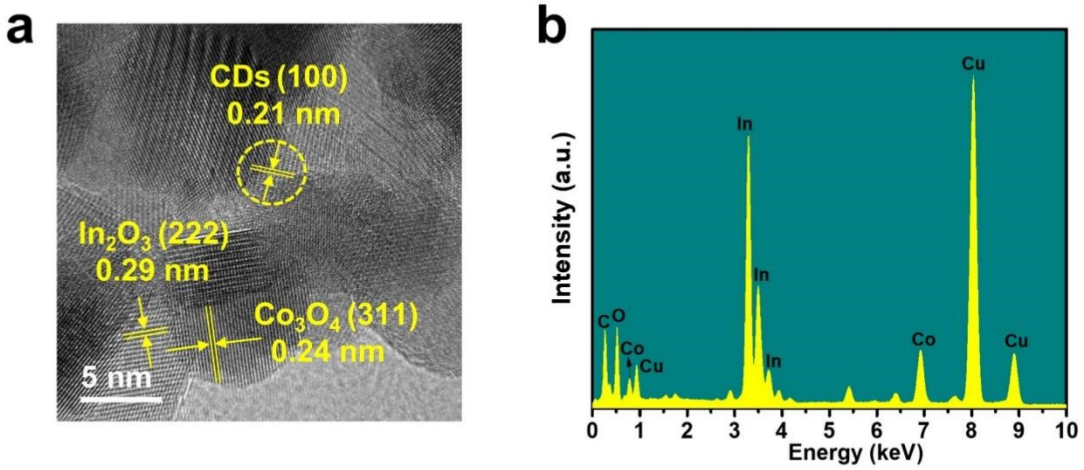

Fig. S3 (a) HRTEM image of CDs-M-CIO, and (b) EDX pattern of 3% CDs-M-CIO.

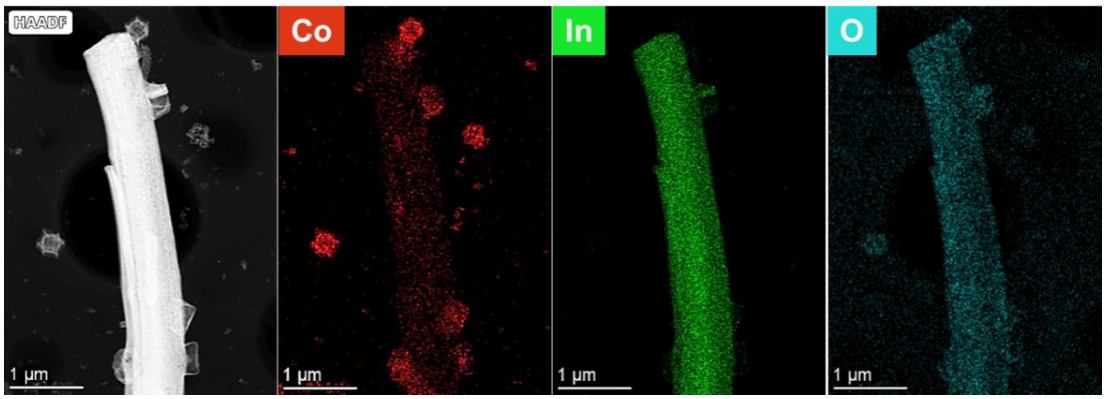

Fig. S4 EDX mapping images of M-Co_3O_4/In_2O_3-550.

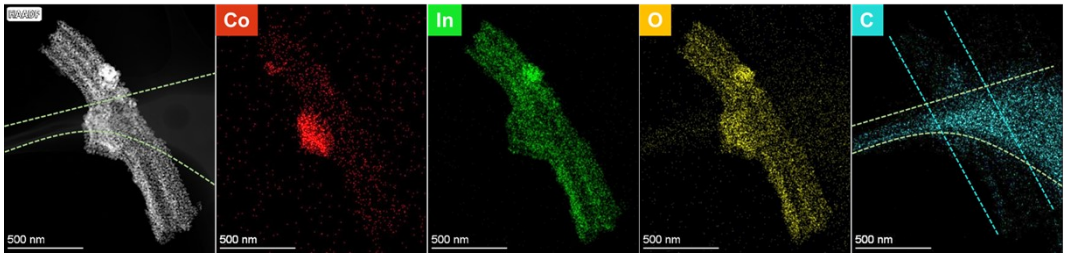

Fig. S5 EDX mapping images of 1% CDs-M-CIO.

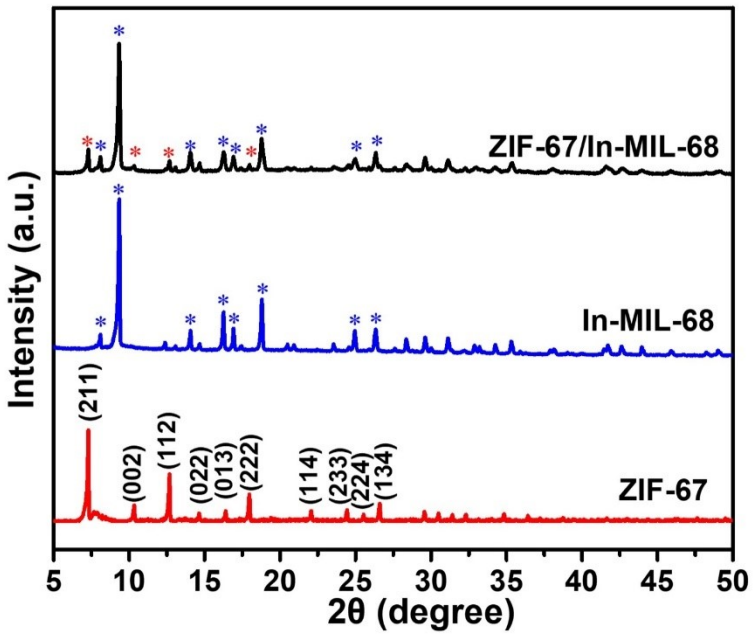

Fig. S6 XRD patterns of MOFs composites.

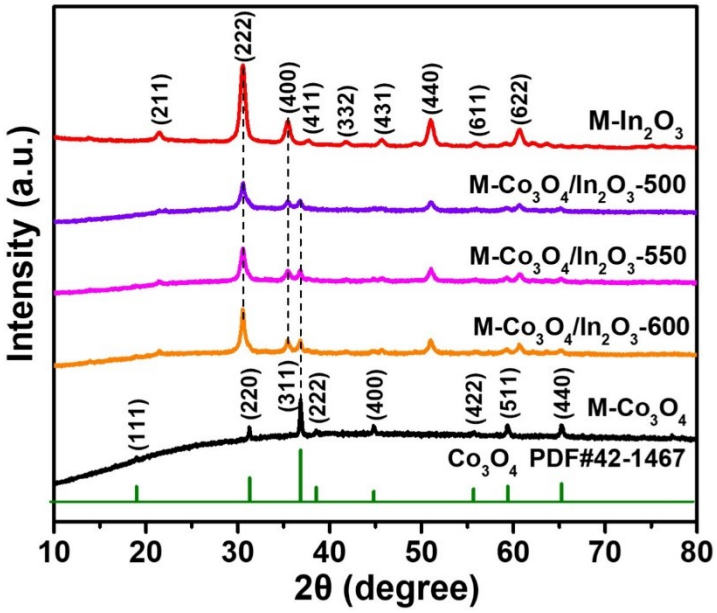

Fig. S7 XRD patterns of M-In_2O_3, M-Co_3O_4 and M-Co_3O_4/In_2O_3 composites.

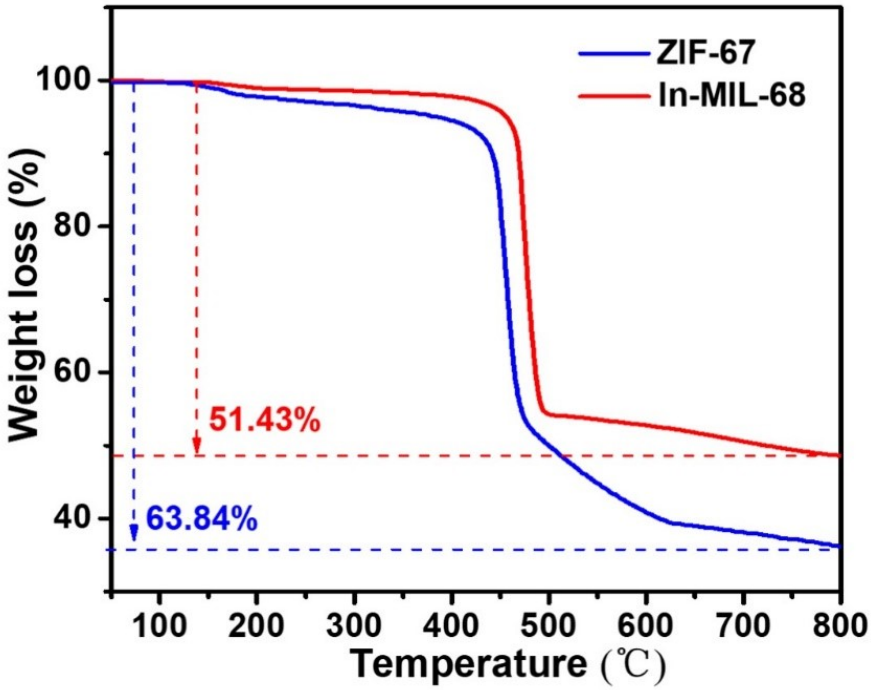

Fig. S8 TGA curves of ZIF-67 and ZIF-67/In-MIL-68 in N_2 atmosphere. The TGA analysis exhibits that the decomposition temperature of ZIF-67 and In-MIL-68 is 480 ^{o}C and 500 ^{o}C, respectively.

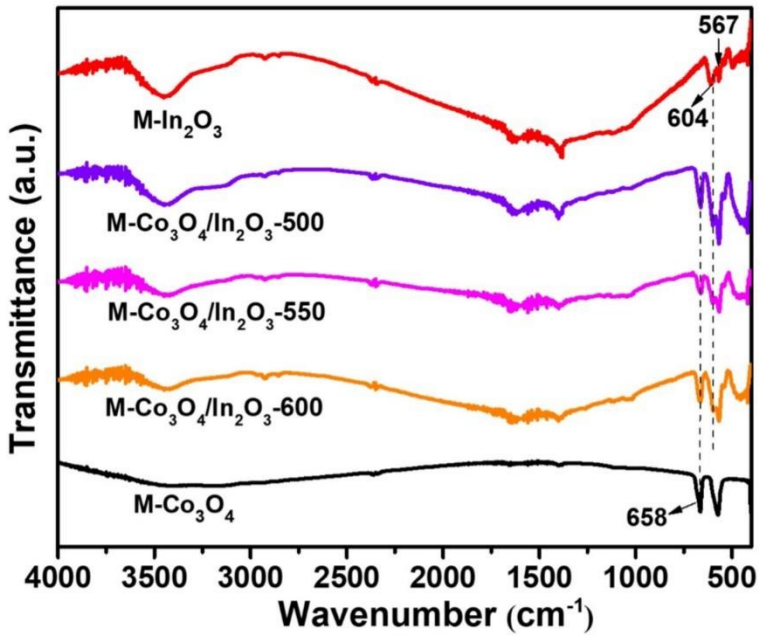

Fig. S9 FT-IR spectra of M-In_2O_3, M-Co_3O_4 and M-Co_3O_4/In_2O_3 composites.

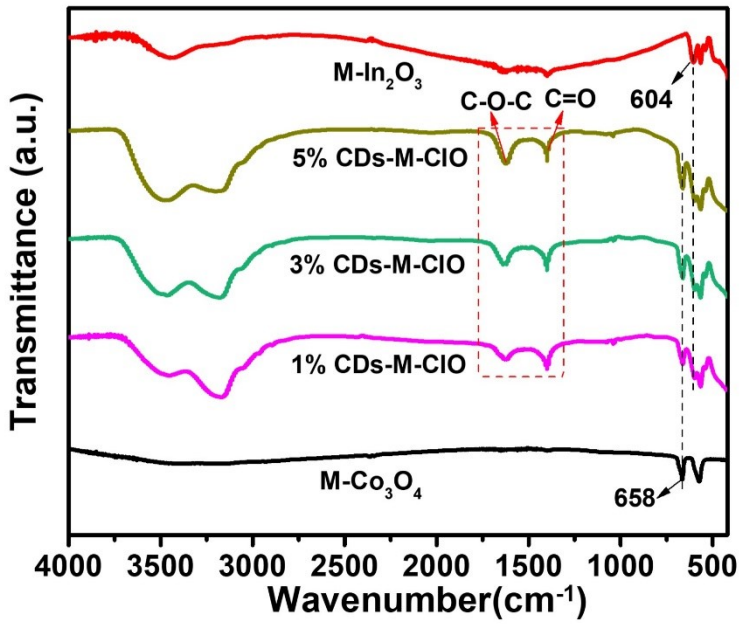

Fig. S10 FT-IR spectra of M-In_2O_3, M-Co_3O_4 and CDs-M-CIO composites.

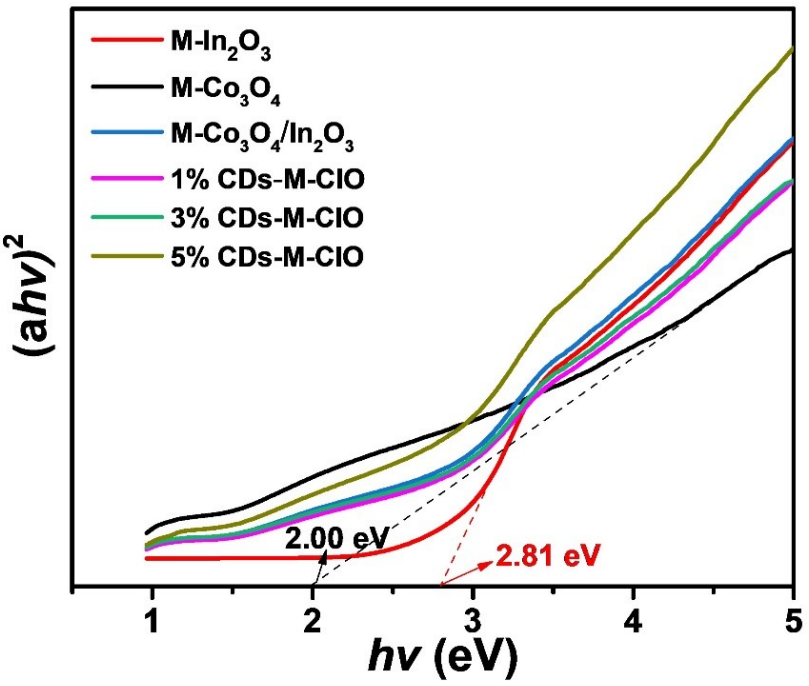

Fig. S11 Tauc plots of the $(ahv)^2$ *versus* photo energy (hv) for M-In_2O_3, M-Co_3O_4, M-Co_3O_4/In_2O_3 and CDs-M-CIO composites.

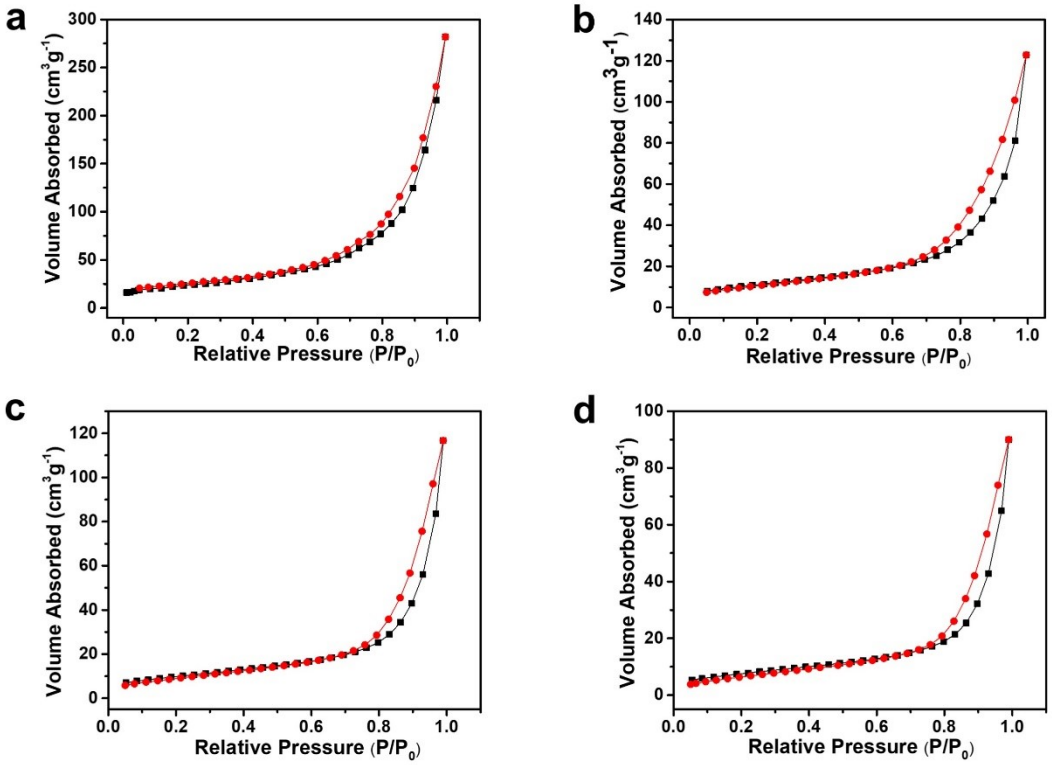

Fig. S12 N_2 adsorption-desorption isotherms of (a) M-In_2O_3, (b) M-Co_3O_4/In_2O_3-550, (c) 3% CDs-M-CIO and (d) M-Co_3O_4.

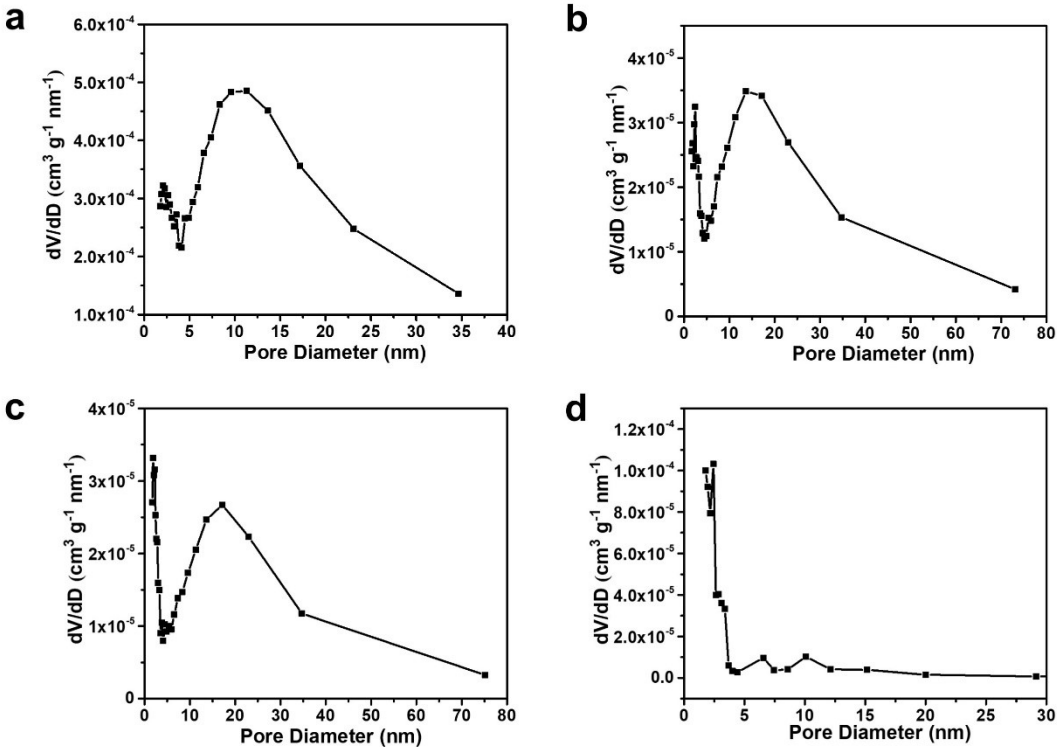

Fig. S13 Pore-size distributions of (a) M-In_2O_3, (b) M-Co_3O_4/In_2O_3-550, (c) 3% CDs-M-CIO and (d) M-Co_3O_4.

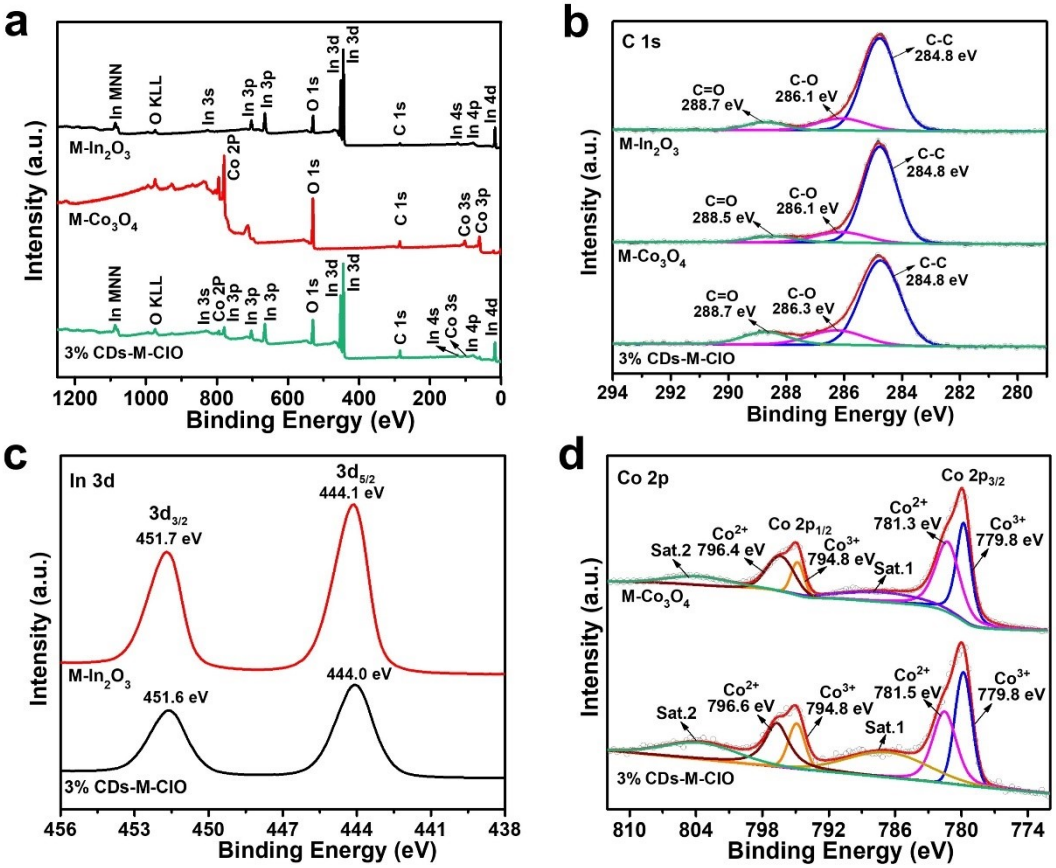

Fig. S14 (a) XPS survey spectra of M-In_2O_3, M-Co_3O_4 and 3% CDs-M-CIO. High resolution XPS spectra of (b) C 1s, (c) In 3d and (d) Co 2p obtained from M-In_2O_3, M-Co_3O_4 and 3% CDs-M-CIO.

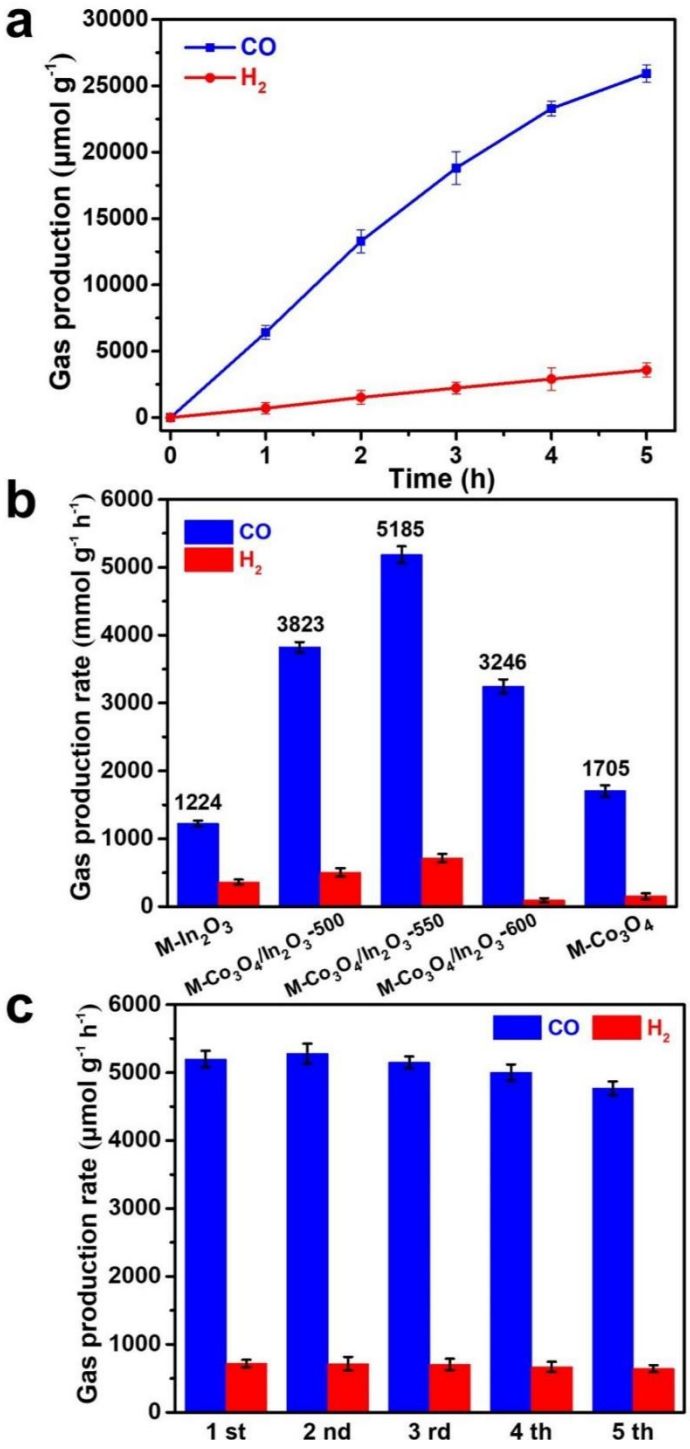

Fig. S15 (a) Photoreduction CO_2 reduction performance of M-Co_3O_4/In_2O_3-550 with $[Ru(bpy)_3]Cl_2$ and TEOA. (b) Gas production rates of different photocatalysts with $[Ru(bpy)_3]Cl_2$ and TEOA. (c) Photocatalytic cycle test of M-Co_3O_4/In_2O_3-550.

The photocatalytic activity of M-Co_3O_4/In_2O_3-x (500, 550, 600 ^oC) was assessed with

$[Ru(bpy)_3]Cl_2$ as the photosensitizer and TEOA as sacrificial agent. For as-prepared samples, the detected gaseous products are CO and a small amount of H_2. M-Co_3O_4/In_2O_3-550 exhibits the maximum CO generation rate of 5185 μmol h^{-1} g^{-1}, which are 4.2 and 3.0 times higher than M-In_2O_3 (1224 μmol h^{-1} g^{-1}) and M-Co_3O_4 (1705 μmol h^{-1} g^{-1}), respectively, suggesting that the intimate contact and p-n heterojunction structure can effectively promote the photocatalytic CO_2 reduction performance. Since the intact In_2O_3 nanotube has a high requirement to calcination temperature, the high or low calcination temperature affects the photocatalytic activity. Further, the photocatalytic stability of M-Co_3O_4/In_2O_3-550 was investigated by recycle experiments. Due to the consumption of photosensitizer and sacrificial agent, the deactivation of CO and H_2 production can be observed after five cycling test.

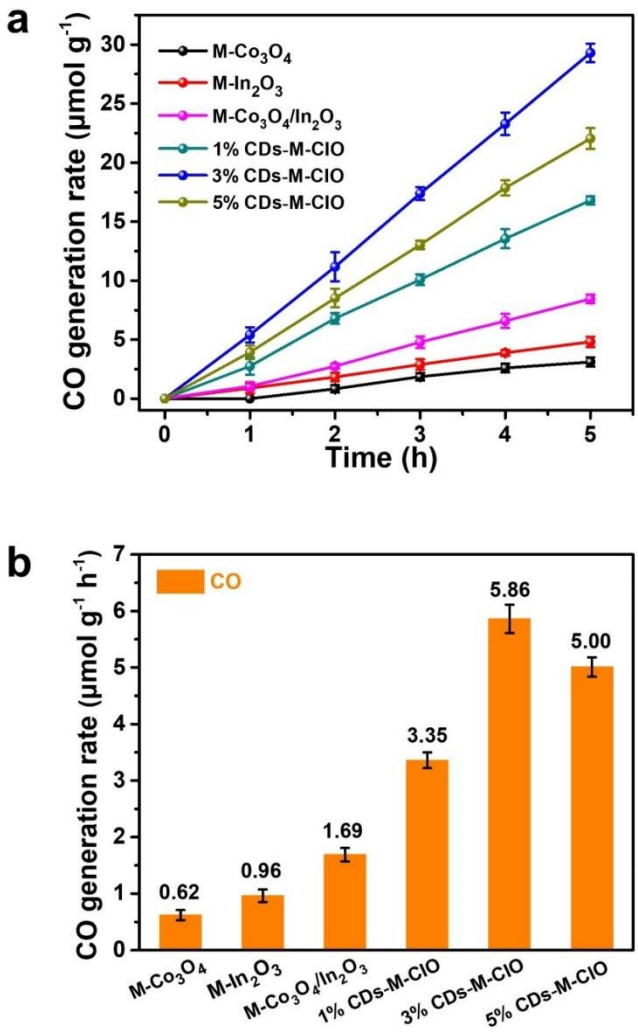

Fig. S16 (a) Photoreduction CO_2 reduction performances of CDs-M-ClO composites with TEOA in absence of $[Ru(bpy)_3]Cl_2$. (b) Gas production rates of different photocatalysts with TEOA in absence of $[Ru(bpy)_3]Cl_2$.

The photocatalytic performance of CDs-based composites is sharp decreased compared with Ru-based composites with the presence of TEOA. It is found that the CO yields of pristine M-Co_3O_4 (0.62 μmol h^{-1} g^{-1}) and M-In_2O_3 (0.96 μmol h^{-1} g^{-1}) are unsatisfactory probably caused by the fast recombination rate, while the M-Co_3O_4/In_2O_3-550 exhibits an enhanced production rate of CO (1.69 μmol h^{-1} g^{-1}). Importantly, the large amounts of CO were generated for CDs-M-ClO composites,

demonstrating that CDs are more conducive to CO_2 reduction. Besides, the optimal proportions of CDs in CDs-M-CIO composites positively affect the CO generation rate. When CDs loading is low (1% CDs-M-CIO), CDs are hard to uniformly disperse on the surface of nanotube, leading to the low charge separation and catalytic performance (1% CDs-M-CIO, CO 3.35 μmol h^{-1} g^{-1}). Predictably, excessive doping CDs can cover the active sites of M-Co_3O_4/In_2O_3 and form the shielding effect, thereby reducing the photocatalytic activity (5% CDs-M-CIO, CO 5.00 μmol h^{-1} g^{-1}).

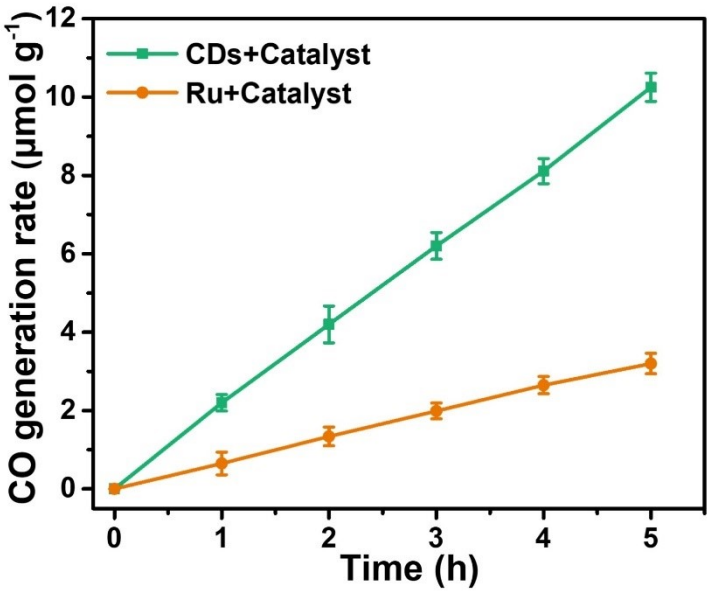

Fig. S17 Photocatalytic CO_2 reduction performances of CDs-catalyst and Ru-catalyst without TEOA as sacrificial agent.

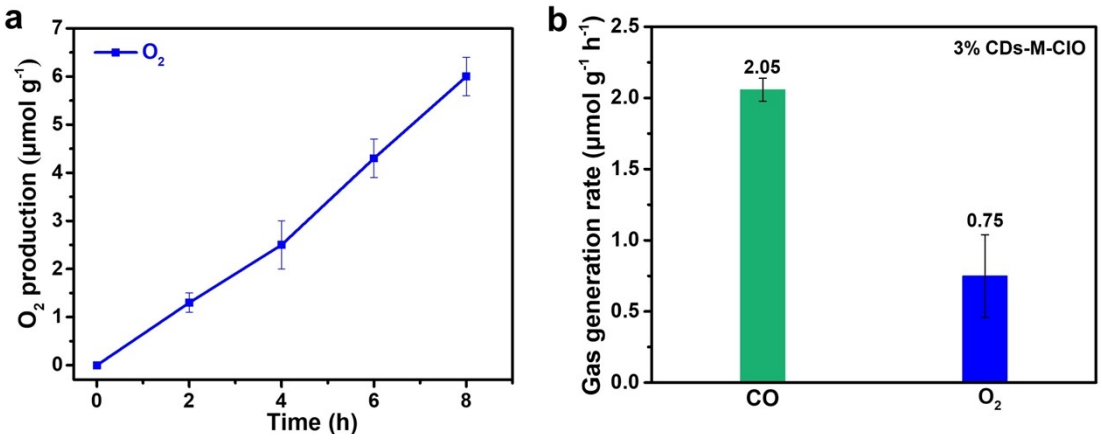

Fig. S18 (a) The time course of O_2 evolution during photocatalytic CO_2 reduction on 3% CDs-M-CIO. (b) Comparation of CO and O_2 evolution rate on 3% CDs-M-CIO. No H_2 amount is detected in the photocatalytic system, suggesting that electrons are mainly consumed by CO_2 reduction instead of H_2 reduction. The photocatalytic CO_2 reduction reactions on CDs-M-CIO can be summarized using the following equations:

$$Co_3O_4\text{-CDs-}In_2O_3 + h\nu \rightarrow Co_3O_4\text{-CDs-}In_2O_3\ (h^+_{VB} + e^-_{CB})$$

$$Co_3O_4\text{-CDs-}In_2O_3\ (h^+_{VB} + e^-_{CB}) \rightarrow Co_3O_4\ (h^+_{VB}) + In_2O_3\ (e^-_{CB})$$

$$Co_3O_4\ (4h^+_{VB}) + 2H_2O \rightarrow O_2 + 4H^+ \qquad E^0_{redox} = +0.82\ V$$

$$In_2O_3\ (4e^-_{CB}) + 2CO_2 + 4H^+ \rightarrow 2CO + 2H_2O \qquad E^0_{redox} = -0.53\ V$$

The reducing CO_2 to CO require two electrons, whereas the formation of O_2 needs four holes. Thus, the theoretical equations indicate that the stoichiometric molar ratio of CO/O_2 should be 2/1. For 3% CDs-M-CIO, the O_2 production rate (0.75 μmol h^{-1} g^{-1}) is slightly lower than half the amount of CO production rate (2.05 μmol h^{-1} g^{-1}), which could be attributed to part of O_2 dissolved in H_2O.

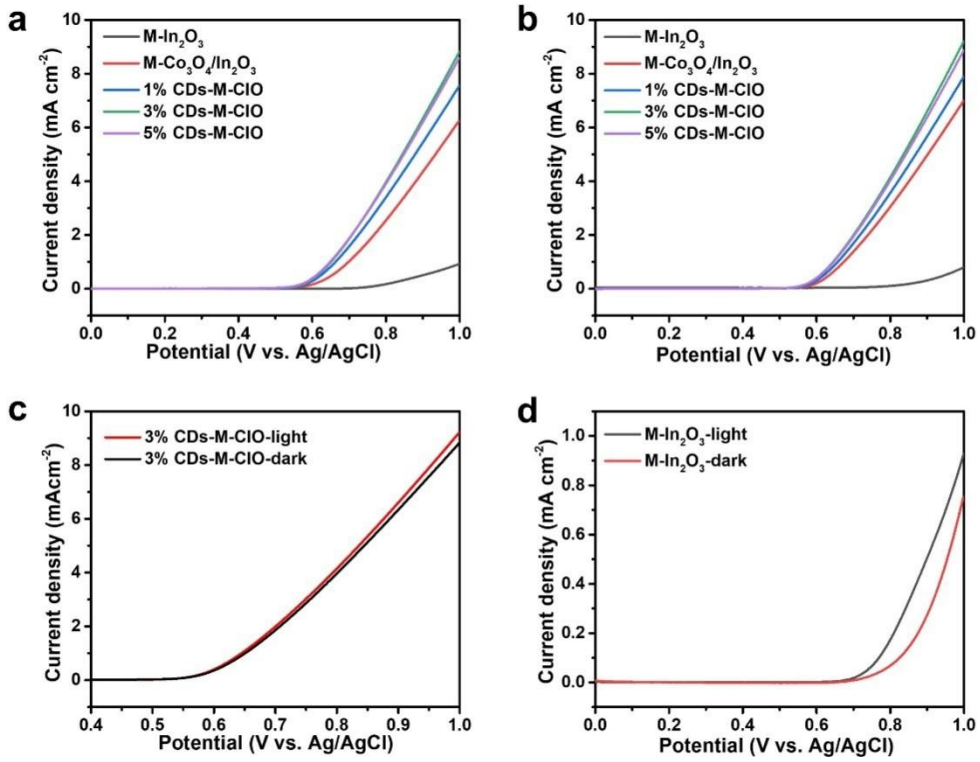

Fig. S19 (a) Polarization curves for as-prepared samples under AM1.5 G sunlight irradiation in 1 M KOH with a scan rate of 5 mV s^{-1}. (b) Polarization curves for as-prepared samples under dark in 1 M KOH with a scan rate of 5 mV s^{-1}. (c) Contrast of polarization curves over 3% CDs-M-ClO under light and dark. (d) Contrast of polarization curves over M-In_2O_3 under light and dark.

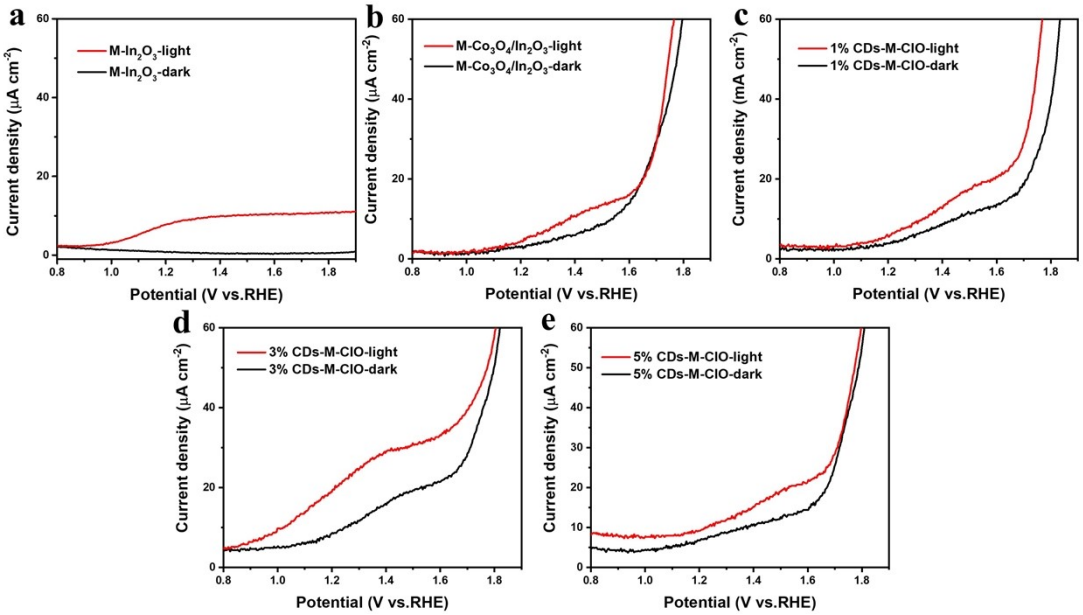

Fig. S20 (a-e) Polarization curves for M-In_2O_3, M-Co_3O_4/In_2O_3 and CDs-M-ClO composites under AM1.5 G sunlight irradiation in Na_2SO_4 with a scan rate of 5 mV s^{-1}.

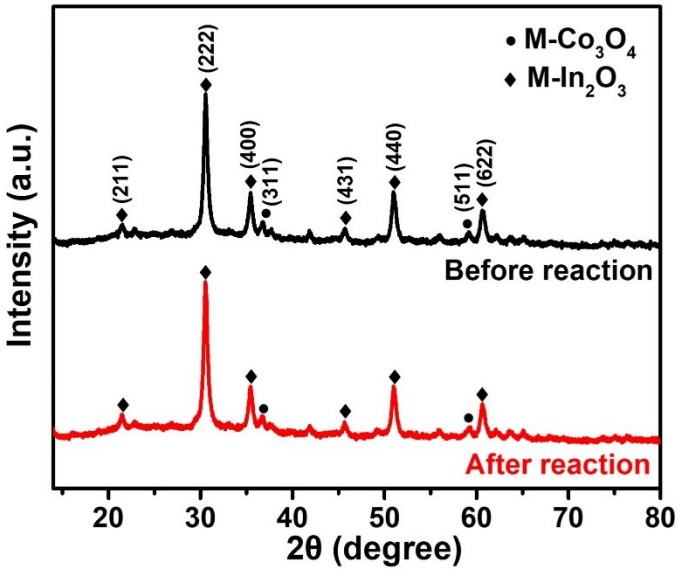

Fig. S21 XRD patterns of 3% CDs-M-CIO composite before and after catalytic reaction.

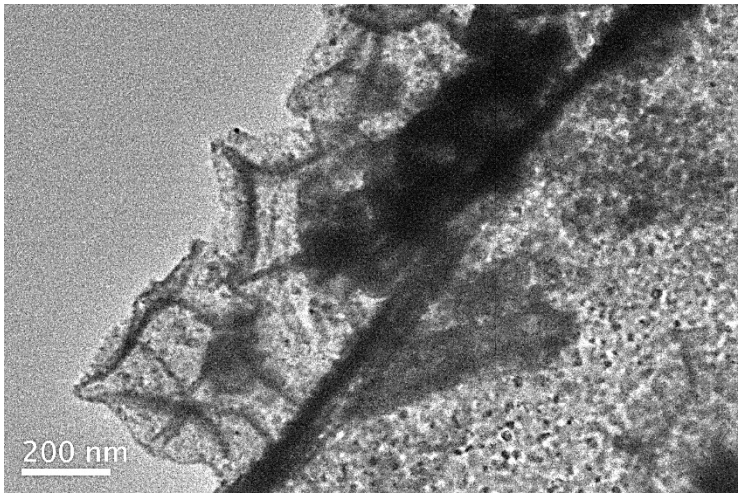

Fig. S22 TEM image of 3% CDs-M-CIO composite after catalytic reaction.

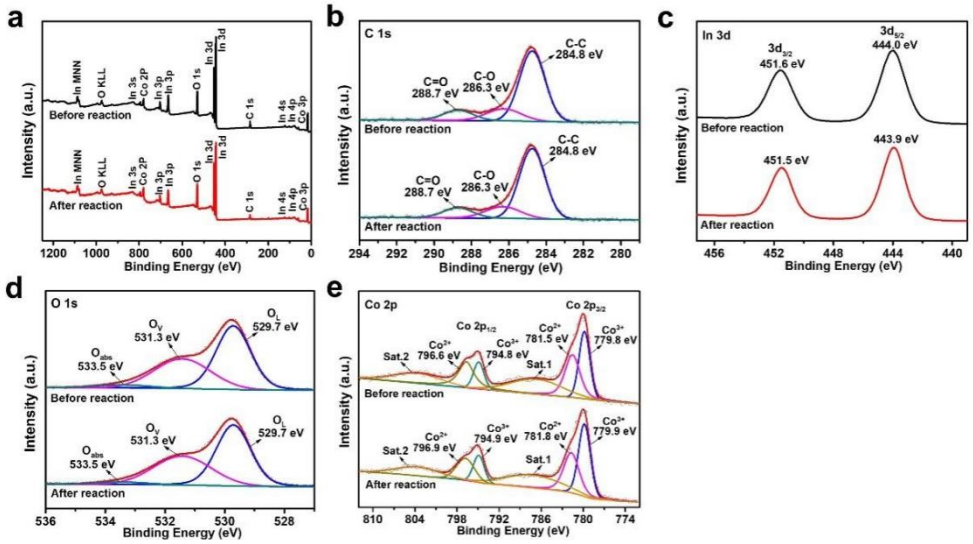

Fig. S23 XPS spectra of 3% CDs-M-CIO composite after cycle reaction.

Supplementary Tables

Table S1. Economic cost of used photosensitizer and sacrificial agent in photocatalytic system.

Material	Product price	Transport price	Total price
$[Ru(bpy)_3]Cl_2$[a]	350 \$ g^{-1}	10 \$ g^{-1}	360 \$ g^{-1}
TEOA[a]	3 \$ g^{-1}	10 \$ g^{-1}	13 \$ g^{-1}
CDs[b]	1.5 \$ g^{-1}	obtained in the lab.	1.5 \$ g^{-1}

[a] Material $[Ru(bpy)_3]Cl_2 \cdot 6H_2O$ (bpy = 2'2-bipyridine) and triethanolamine (TEOA) were purchased from Sigma-Aldrich at current prices. The price difference could be existed in different region. [b] The price of CDs is calculated as follows. The price of one graphite rod is about 1.5 \$ (3 g per rod). Based on the power condition (30 V bias, 2 A current), 0.06 kilowatt-hour of electricity is consumed every day, and the preparation process usually need 10 days. The price of one kilowatt-hour in China is 0.5-0.6 ¥ (about 0.09 \$ per kilowatt-hour), and therefore, the price of used electricity is around 0.054 \$. In the whole process, manpower is seldom used, and the cost of manpower can be negligible. Two graphite rods (about 6 g) can generate about 2 g CDs, and thus the price of CDs is 1.5 \$ g^{-1}.

Table S2. Porous characteristics of as-prepared samples.

Sample	S_{BET} (m^2 g^{-1})	$S_{Langmuir}$ (m^2 g^{-1})	Pore volume (cm^3 g^{-1})	Pore size (nm)
M-In_2O_3	87.52	215.74	0.38	18.59
M-Co_3O_4/In_2O_3-550	52.27	174.26	0.21	22.76
3% CDs-M-CIO	43.84	125.18	0.18	25.52
M-Co_3O_4	25.63	82.91	0.14	15.28

Table S3. Comparison of similar photocatalytic systems for CO_2 reduction performance presented in recent papers.

Photocatalyst	Photosensitizer	Sacrificial agent	Solvent	Light source	Production rate (μmol g^{-1} h^{-1})			Reference
					CO	CH_4	H_2	
M-Co_3O_4/In_2O_3-550	[Ru(bpy)$_3$]Cl_2·$6H_2O$	TEOA	MeCN/H_2O (4:1 v/v)	AM1.5G	5185	/	716	This work
3% CDs-M-CIO	/	/	MeCN/H_2O (4:1 v/v)	AM1.5G	2.06	/	/	This work
Co_3O_4 HPS	[Ru(bpy)$_3$]Cl_2·$6H_2O$	TEOA	MeCN/H_2O (3:1 v/v)	λ >420 nm	2003	/	595	1
Co_3O_4 HNSs	[Ru(bpy)$_3$]Cl_2·$6H_2O$	TEOA	MeCN/H_2O (3:1 v/v)	λ >400 nm	1985	/	583	2
Co_3O_4-NS	[Ru(bpy)$_3$]Cl_2·$6H_2O$	TEOA	MeCN/H_2O (3:2 v/v)	λ >400 nm	90.4	/	38.6	3
$ZnIn_2S_4$-In_2O_3	$Co(bpy)_3^{2+}$	TEOA	MeCN/H_2O (3:2 v/v)	λ >400 nm	3075	/	800	4
C-In_2O_3	Pt	TEOA	H2O	300 W Xe lamp	126.6	27.9	/	5
1.0-In_2O_3	Pt	/	H_2O vapor	500 W Hg lamp	1.43	3.5	/	6
Co-OMT-4	/	/	CO_2/H_2O vapor	λ > 420 nm	1.94	0.09	/	7
Cu_2O/TiO_2	/	/	CO_2/H_2O vapor	Hg arc lamp, λ ≥ 305 nm	2.11	/	/	8
Fe_2O_3/Cu_2O	/	/	CO_2/H_2O vapor	λ >400 nm	1.67	/	/	9

Supplementary References

[1] C. Gao, Q. Meng, K. Zhao, H. Yin, D. Wang, J. Guo, S. Zhao, L. Chang, M. He, Q. Li, H. Zhao, X. Huang, Y. Cao and Z. Tang, *Adv. Mater.,* 2016, **28**, 6485-6490.

[2] J.-T. Ren, Y.-L. Zheng, K. Yuan, L. Zhou, K. Wu and Y.-W. Zhang, *Nanoscale,* 2020, **12**, 755-762.

[3] W. Chen, B. Han, C. Tian, X. Liu, S. Liang, H. Deng, Z. Lin, *Appl. Catal. B,* 2019, **244**, 996-1003.

[4] S. Wang, B. Y. Guan and X. W. Lou, *J. Am. Chem. Soc.,* 2018, **140**, 5037-5040.

[5] Y.-X. Pan, Y. You, S. Xin, Y. Li, G. Fu, Z. Cui, Y.-L. Men, F.-F. Cao, S.-H. Yu and J. B. Goodenough, *J. Am. Chem. Soc.,* 2017, **139,** 4123-4129.

[6] Y. Wang, J. Zhao, Y. Li and C. Wang, *Appl. Catal. B,* 2018, **226**, 544-553.

[7] T. Wang, X. Meng, G. Liu, K. Chang, P. Li, Q. Kang, L. Liu, M. Li, S. Ouyang and J. Ye, *J. Mater. Chem. A,* 2015, **3,** 9491-9501.

[8] M. E. Aguirre, R. Zhou, A. J. Eugene, M. I. Guzman and M. A. Grela, *Appl. Catal. B,* 2017, **217**, 485-493.

[9] J.-C. Wang, L. Zhang, W.-X. Fang, J. Ren, Y.-Y. Li, H.-C. Yao, J.-S. Wang, Z.-J. Li, *ACS Appl. Mater. Interfaces,* 2015, **7**, 8631-8639.